AIAA Paper 2004-2240, 2004

Flutter Prediction Based on Fully Coupled Fluid-Structural Interactions

Xiangying Chen, Ge-Cheng Zha and Zongjun Hu

Dept. of Mechanical and Aerospace Engineering
University of Miami
Coral Gables, Florida 33124

Background

- Fully coupled fluid-structure model is necessary to capture the nonlinear flow phenomena and structure coupling for turbomachinery flow induced vibration

- e.g.: Stall flutter have unsteady flow separation, shock motion, oscillating tip vortex, blade coupling in a bladed disk (IBR).

- Prescribed blade motion is difficult (inaccurate) if not impossible

- Final goal: develop high fidelity prediction tool for mistunned bladed disk flutter prediction

CFD Aerodynamic Model

- Reynolds-Averaged Navier-Stokes equations(RANS)

$$\frac{\partial \mathbf{Q}'}{\partial \tau} + \frac{\partial \mathbf{Q}'}{\partial t} + \frac{\partial \mathbf{E}'}{\partial \xi} + \frac{\partial \mathbf{F}'}{\partial \eta} + \frac{\partial \mathbf{G}'}{\partial \zeta} = \frac{1}{Re}\left(\frac{\partial \mathbf{E}'_{\mathbf{v}}}{\partial \xi} + \frac{\partial \mathbf{F}'_{\mathbf{v}}}{\partial \eta} + \frac{\partial \mathbf{G}'_{\mathbf{v}}}{\partial \zeta}\right) \tag{1}$$

$$\mathbf{Q}' = \frac{\mathbf{Q}}{J} \tag{2}$$

$$\mathbf{E}' = \frac{1}{J}(\xi_t \mathbf{Q} + \xi_x \mathbf{E} + \xi_y \mathbf{F} + \xi_z \mathbf{G}) = \frac{1}{J}(\xi_t \mathbf{Q} + \mathbf{E}'') \tag{3}$$

$$\mathbf{F}' = \frac{1}{J}(\eta_t \mathbf{Q} + \eta_x \mathbf{E} + \eta_y \mathbf{F} + \eta_z \mathbf{G}) = \frac{1}{J}(\eta_t \mathbf{Q} + \mathbf{F}'') \tag{4}$$

$$\mathbf{G}' = \frac{1}{J}(\zeta_t \mathbf{Q} + \zeta_x \mathbf{E} + \zeta_y \mathbf{F} + \zeta_z \mathbf{G}) = \frac{1}{J}(\zeta_t \mathbf{Q} + \mathbf{G}'') \tag{5}$$

$$\mathbf{E}'_{\mathbf{v}} = \frac{1}{J}(\xi_x \mathbf{E}_{\mathbf{v}} + \xi_y \mathbf{F}_{\mathbf{v}} + \xi_z \mathbf{G}_{\mathbf{v}}) \tag{6}$$

$$\mathbf{F}'_{\mathbf{v}} = \frac{1}{J}(\eta_x \mathbf{E}_{\mathbf{v}} + \eta_y \mathbf{F}_{\mathbf{v}} + \eta_z \mathbf{G}_{\mathbf{v}}) \tag{7}$$

$$\mathbf{G}'_{\mathbf{v}} = \frac{1}{J}(\zeta_x \mathbf{E}_{\mathbf{v}} + \zeta_y \mathbf{F}_{\mathbf{v}} + \zeta_z \mathbf{G}_{\mathbf{v}}) \tag{8}$$

$$\mathbf{Q} = \begin{pmatrix} \bar{\rho} \\ \bar{\rho}\tilde{u} \\ \bar{\rho}\tilde{v} \\ \bar{\rho}\tilde{w} \\ \bar{\rho}\tilde{e} \end{pmatrix}, \; \mathbf{E} = \begin{pmatrix} \bar{\rho}\tilde{u} \\ \bar{\rho}\tilde{u}\tilde{u} + \tilde{p} \\ \bar{\rho}\tilde{u}\tilde{v} \\ \bar{\rho}\tilde{u}\tilde{w} \\ (\bar{\rho}\tilde{e} + \tilde{p})\tilde{u} \end{pmatrix},$$
$$\mathbf{F} = \begin{pmatrix} \bar{\rho}\tilde{v} \\ \bar{\rho}\tilde{u}\tilde{v} \\ \bar{\rho}\tilde{v}\tilde{v} + \tilde{p} \\ \bar{\rho}\tilde{w}\tilde{v} \\ (\bar{\rho}\tilde{e} + \tilde{p})\tilde{v} \end{pmatrix}, \; \mathbf{G} = \begin{pmatrix} \bar{\rho}w \\ \bar{\rho}\tilde{u}\tilde{w} \\ \bar{\rho}\tilde{v}\tilde{w} \\ \bar{\rho}\tilde{w}\tilde{w} + \tilde{p} \\ (\bar{\rho}\tilde{e} + \tilde{p})\tilde{w} \end{pmatrix},$$

$$\mathbf{E}'' = \xi_x \mathbf{E} + \xi_y \mathbf{F} + \xi_z \mathbf{G},$$

$$\mathbf{F}'' = \eta_x \mathbf{E} + \eta_y \mathbf{F} + \eta_z \mathbf{G},$$

$$\mathbf{G}'' = \zeta_x \mathbf{E} + \zeta_y \mathbf{F} + \zeta_z \mathbf{G},$$

$$\mathbf{E_v} = \begin{pmatrix} 0 \\ \bar{\tau}_{xx} - \overline{\rho u'' u''} \\ \bar{\tau}_{xy} - \overline{\rho u'' v''} \\ \bar{\tau}_{xz} - \overline{\rho u'' w''} \\ Q_x \end{pmatrix}, \mathbf{F_v} = \begin{pmatrix} 0 \\ \bar{\tau}_{yx} - \overline{\rho v'' u''} \\ \bar{\tau}_{yy} - \overline{\rho v'' v''} \\ \bar{\tau}_{yz} - \overline{\rho v'' w''} \\ Q_y \end{pmatrix},$$
$$\mathbf{G_v} = \begin{pmatrix} 0 \\ \bar{\tau}_{zx} - \overline{\rho w'' u''} \\ \bar{\tau}_{zy} - \overline{\rho w'' v''} \\ \bar{\tau}_{zz} - \overline{\rho w'' w''} \\ Q_z \end{pmatrix}$$

$$\bar{\tau}_{ij} = -\frac{2}{3}\tilde{\mu}\frac{\partial \tilde{u}_k}{\partial x_k}\delta_{ij} + \tilde{\mu}(\frac{\partial \tilde{u}_i}{\partial x_j} + \frac{\partial \tilde{u}_j}{\partial x_i}) \tag{9}$$

$$Q_i = \tilde{u}_j(\bar{\tau}_{ij} - \overline{\rho u'' u''}) - (\bar{q}_i + C_p\overline{\rho T'' u_i''}) \tag{10}$$

$$\bar{q}_i = -\frac{\tilde{\mu}}{(\gamma - 1)Pr}\frac{\partial a^2}{\partial x_i} \tag{11}$$

- Molecular viscosity $\tilde{\mu} = \tilde{\mu}(\tilde{T})$ is determined by Sutherland law

- Speed of sound $a = \sqrt{\gamma R T_\infty}$

- Total energy:

$$\bar{\rho}\tilde{e} = \frac{\tilde{p}}{(\gamma - 1)} + \frac{1}{2}\bar{\rho}(\tilde{u}^2 + \tilde{v}^2 + \tilde{w}^2) + k \tag{12}$$

- Turbulent shear stresses and heat flux are calculated
by Baldwin-Lomax model

Time Marching Scheme

Implicit unfactored line Gauss-Seidel iteration, dual time stepping

$$[(\frac{1}{\Delta\tau} + \frac{1.5}{\Delta t})I - (\frac{\partial R}{\partial Q})^{n+1,m}]\delta Q^{n+1,m+1} = R^{n+1,m} - \frac{3Q^{n+1,m} - 4Q^{n} + Q^{n-1}}{2\Delta t} \tag{13}$$

$$R = -\frac{1}{V}\int_s [(F - F_v)\mathbf{i} + (G - G_v)\mathbf{j} + (H - H_v)\mathbf{k}]\cdot d\mathbf{s} \tag{14}$$

Roe's Riemann Solver on Moving Grid System

$$\mathbf{E}'_{i+\frac{1}{2}} = \frac{1}{2}[\mathbf{E}''(\mathbf{Q_L})+\mathbf{E}''(\mathbf{Q_R})+\mathbf{Q_L}\xi_{tL}+\mathbf{Q_R}\xi_{tR}-|\tilde{\mathbf{A}}|(\mathbf{Q_R}-\mathbf{Q_L})]_{i+\frac{1}{2}} \tag{15}$$

$$\tilde{\mathbf{A}} = \tilde{\mathbf{T}}\tilde{\mathbf{\Lambda}}\tilde{\mathbf{T}}^{-1} \tag{16}$$

$$(\tilde{U}+\tilde{C}, \tilde{U}-\tilde{C}, \tilde{U}, \tilde{U}, \tilde{U}) \tag{17}$$

$$\tilde{U} = \tilde{\xi}_t + \xi_x\tilde{u} + \xi_y\tilde{v} + \xi_z\tilde{w} \tag{18}$$

$$\tilde{C} = \tilde{c}\sqrt{\xi_x^2+\xi_y^2+\xi_z^2} \tag{19}$$

$$\tilde{\xi}_t = (\xi_{tL} + \xi_{tR}\sqrt{\rho_R/\rho_L})/(1+\sqrt{\rho_R/\rho_L}) \tag{20}$$

Boundary Conditions

• Upstream boundary conditions: All the variables are specified using freestream condition except the pressure is extrapolated from interior

• Downstream boundary conditions: All the variables are extrapolated from interior except the pressure is set to be its freestream value

• Solid wall boundary conditions: Non-slip condition

$$u_0 = 2\dot{x}_b - u_1, \qquad v_0 = 2\dot{y}_b - v_1 \tag{21}$$

and adiabatic and the inviscid normal momentum equation

$$\frac{\partial T}{\partial \eta} = 0, \quad \frac{\partial p}{\partial \eta} = -\left(\frac{\rho}{\eta_x^2 + \eta_y^2}\right)(\eta_x \ddot{x}_b + \eta_y \ddot{y}_b) \tag{22}$$

Geometric Conservation Law

$$\mathbf{S} = \mathbf{Q}\left[\frac{\partial J^{-1}}{\partial t} + \left(\frac{\xi_t}{J}\right)_\xi + \left(\frac{\eta_t}{J}\right)_\eta + \left(\frac{\zeta_t}{J}\right)_\zeta\right] \tag{23}$$

$$\mathbf{S}^{n+1} = \mathbf{S}^n + \frac{\partial \mathbf{S}}{\partial \mathbf{Q}}\Delta\mathbf{Q}^{n+1} \tag{24}$$

Structural model for elastic cylinder:

$$m\ddot{x} + C_x\dot{x} + K_x x = D \tag{25}$$

$$m\ddot{y} + C_y\dot{y} + K_y y = L \tag{26}$$

$C_x = C_y$ and $K_x = K_y$, After normalization:

$$\ddot{x} + 2\zeta\left(\frac{2}{\bar{u}}\right)\dot{x} + \left(\frac{2}{\bar{u}}\right)^2 x = \frac{2}{\mu_s \pi} C_d \tag{27}$$

$$\ddot{y} + 2\zeta\left(\frac{2}{\bar{u}}\right)\dot{y} + \left(\frac{2}{\bar{u}}\right)^2 y = \frac{2}{\mu_s \pi} C_l \tag{28}$$

$\zeta = \frac{C_{x,y}}{2\sqrt{mK_{x,y}}}$, $\bar{u} = \frac{U_\infty}{b\omega}$, $b = r$, $\omega = \sqrt{K_{x,y}/m}$, $\mu_s = \frac{m}{\pi \rho_\infty b^2}$,
C_d and C_l = Lift and drag coefficient

Matrix form:

$$[\mathbf{M}]\frac{\partial\{\mathbf{S}\}}{\partial t} + [\mathbf{K}]\{\mathbf{S}\} = \mathbf{q} \tag{29}$$

where

$$\mathbf{S} = \begin{pmatrix} x \\ \dot{x} \\ y \\ \dot{y} \end{pmatrix}, \mathbf{M} = [I],$$

$$\mathbf{K} = \begin{pmatrix} 0 & -1 & 0 & 0 \\ \left(\frac{2}{\bar{u}}\right)^2 & 2\zeta\left(\frac{2}{\bar{u}}\right) & 0 & 0 \\ 0 & 0 & 0 & -1 \\ 0 & 0 & \left(\frac{2}{\bar{u}}\right)^2 & 2\zeta\left(\frac{2}{\bar{u}}\right) \end{pmatrix}, \mathbf{q} = \begin{pmatrix} 0 \\ \frac{2}{\mu_s\pi}C_d \\ 0 \\ \frac{2}{\mu_s\pi}C_l \end{pmatrix}.$$

Time Marching:

$$\left(\frac{1}{\Delta\tau}\mathbf{I} + \frac{1.5}{\Delta t}\mathbf{M} + \mathbf{K}\right)\delta S^{n+1,m+1} = -\mathbf{M}\frac{3\mathbf{S}^{n+1,m} - 4\mathbf{S}^{n} + \mathbf{S}^{n-1}}{2\Delta t} - \mathbf{K}\mathbf{S}^{n+1,m} + \mathbf{q}^{n+1,m+1} \tag{30}$$

Structural model for elastic airfoil:

$$m\ddot{h} + S_\alpha \ddot{\alpha} + K_h h = -L \tag{31}$$
$$S_\alpha \ddot{h} + I_\alpha \ddot{\alpha} + K_\alpha \alpha = M \tag{32}$$

Normalized:

$$\ddot{h} + x_\alpha \ddot{\alpha} + \left(\frac{\omega_h}{\omega_\alpha}\right)^2 h = -\frac{U^{*2}}{\mu\pi} C_l \tag{33}$$
$$x_\alpha \ddot{h} + r_\alpha^2 \ddot{\alpha} + r_\alpha^2 \alpha = \frac{U^{*2}}{\mu\pi} C_m \tag{34}$$

$U^* = \frac{U_\infty}{\omega_\alpha b}$,

Time scale: $t_s^* = \frac{\omega_\alpha L}{U_\infty} t_f^*$

Fully Coupled Fluid-Structural Interaction Procedure

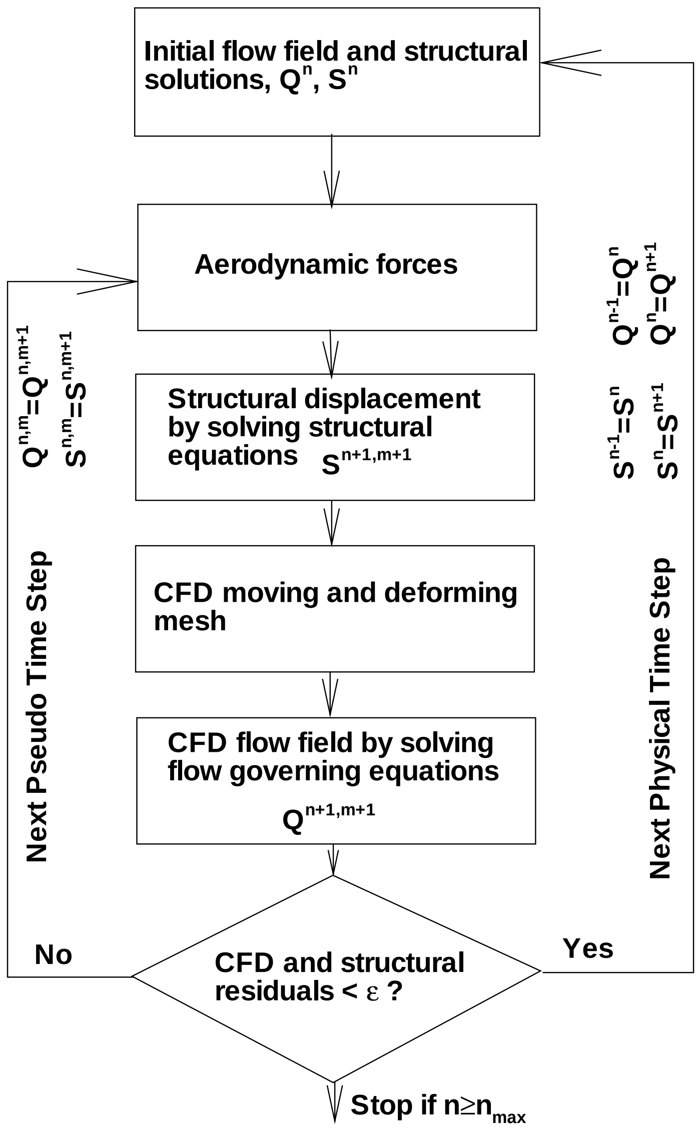

Figure 1: Flow-Structure Interaction Calculation Steps

- **Mesh Deformation Strategy**

1) inner zone: moving with the solid object, not deformed, keep the orthogonality and save CPU time

2) outer zone: moved with inner zone, deformed as a spring system, far field boundary stationary

Vortex-Induced Oscillating Cylinder

Re=500, M=0.2

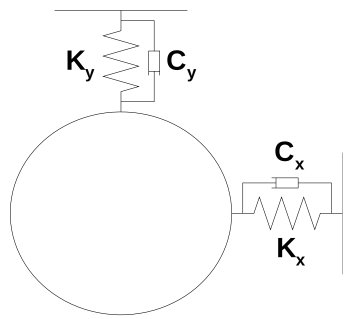

Figure 2: Sketch of the elastically mounted cylinder

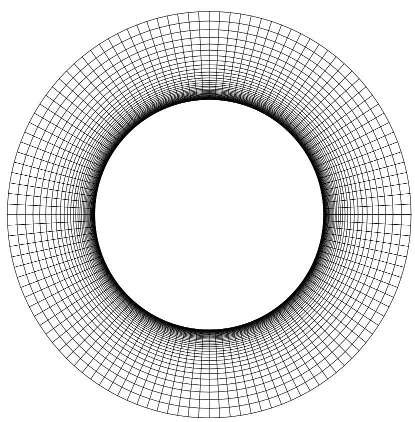

Figure 3: Mesh around the cylinder near the solid surface

Validation of Stationary cylinder vortex shedding

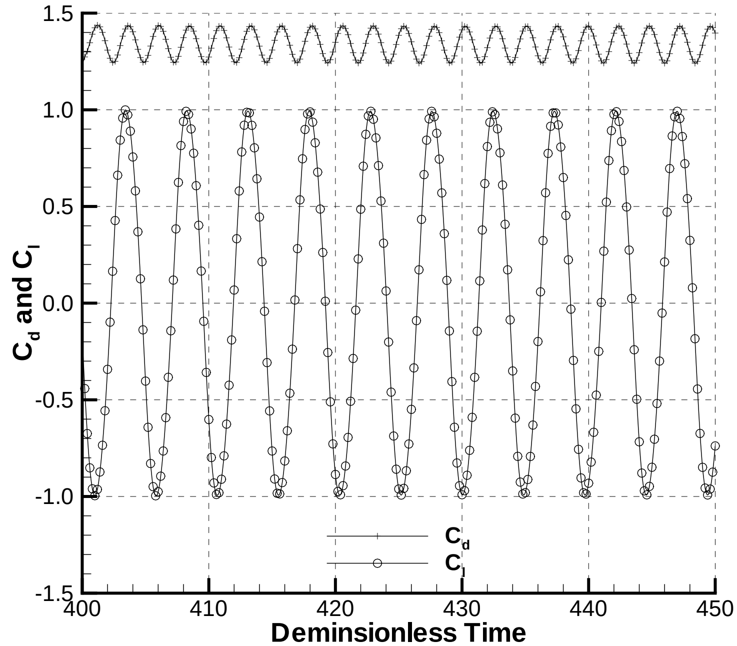

Figure 4: Time history of the lift and drag of the stationary cylinder due to vortex shedding

Table 1: Results of Mesh Refinement Study and comparison with the experiments

Mesh Dimension	St_{C_d}	St_{C_l}	St_{C_m}	C_l	C_d
80×40	0.3931	0.1978	0.1978	±1.0164	1.3415±0.0916
120×80	0.4126	0.2075	0.2075	±0.9921	1.3405±0.0958
200×150	0.4199	0.2100	0.2100	±0.9994	1.3525±0.0989
(Roshko 1954)		0.2075			
(Goldstein 1938)		0.2066			
384×96 (Alonso 1995)	0.46735	0.23313		1.14946(C_{lmax})	1.31523(C_{davg})

Flow induced vibration

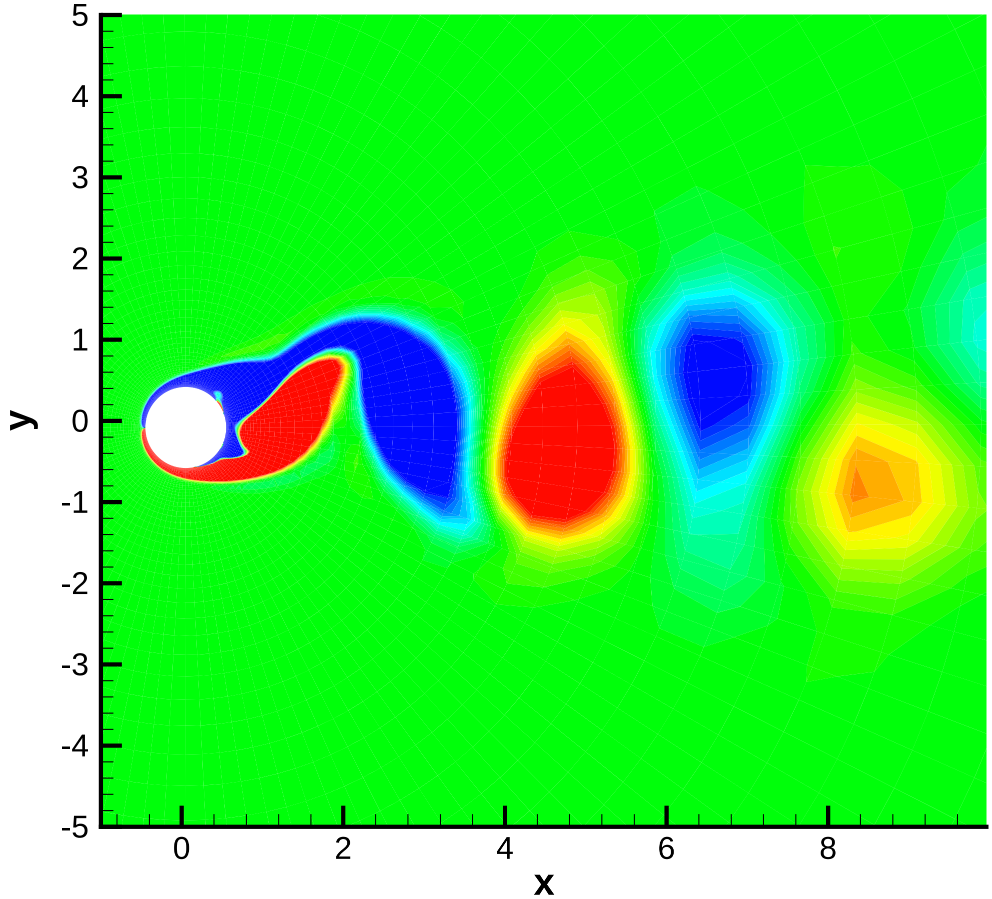

Figure 5: Vorticity contours with small cylinder structural oscillation amplitude, $\mu_s = 12.7324$, $\zeta = 0.1583$,

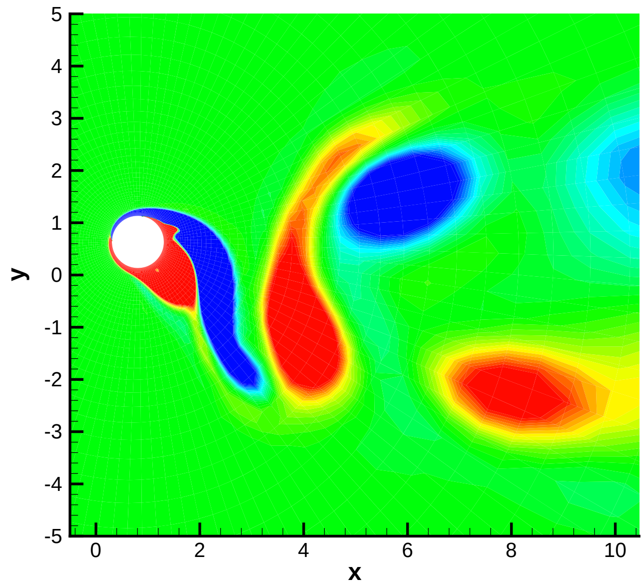

Figure 6: Vorticity contours with large cylinder structural oscillation amplitude, $\mu_s = 1.2732$, $\zeta = 0.01583$

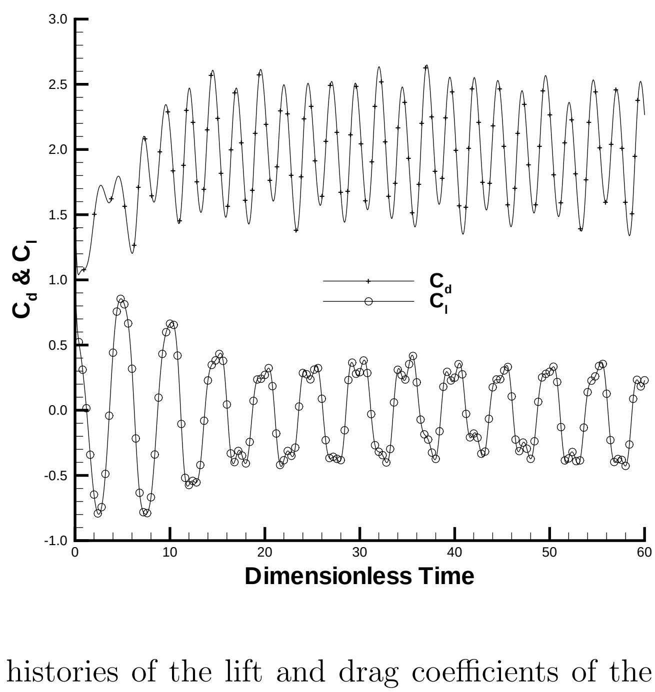

Figure 7: Time histories of the lift and drag coefficients of the oscillating cylinder, $\mu_s = 5$, $\zeta = 0.0403$

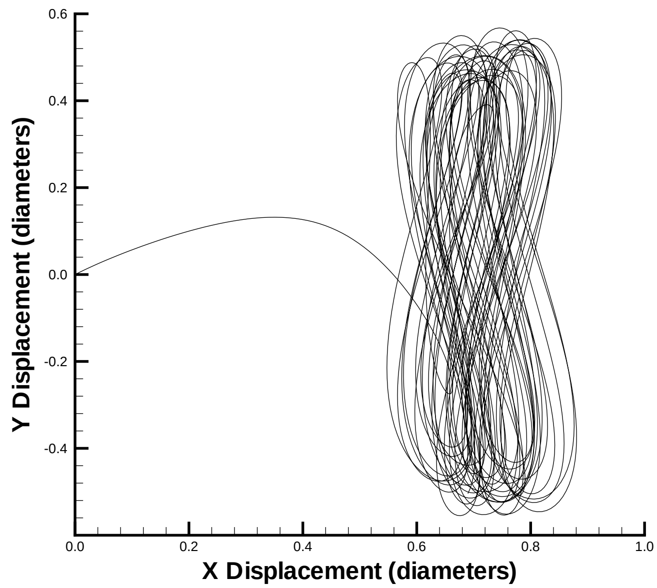

Figure 8: The trajectory of the Time histories of the lift and drag coefficients of the oscillating cylinder, $\mu_s = 1.2732$, $\zeta = 0.1583$

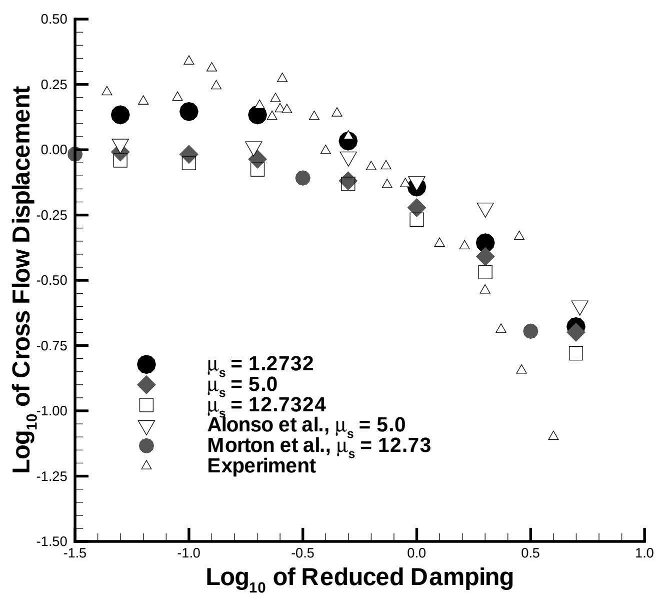

Figure 9: Comparison of the computed amplitude with Griffin's experimental data for the elastically mounted cylinder.

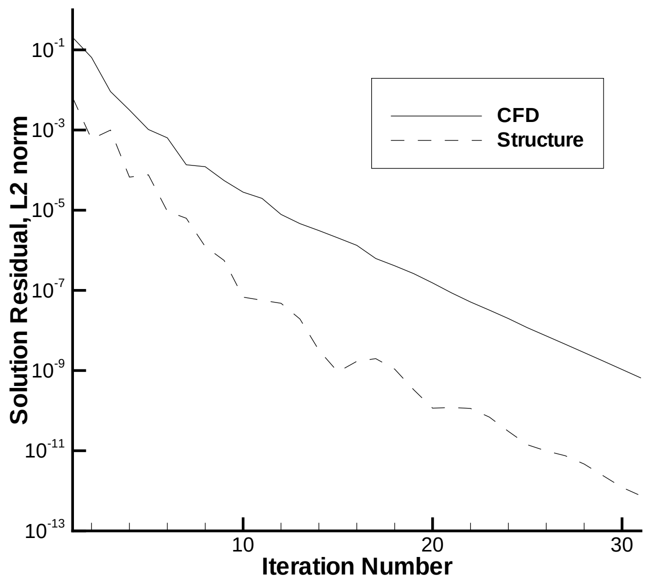

Figure 10: Convergence histories for both CFD and structural solvers within one physical time step

Steady State Flow of Transonic RAE 2822 Airfoil

Re=6.5×10^6, M_∞=0.729, AoA=2.31°.

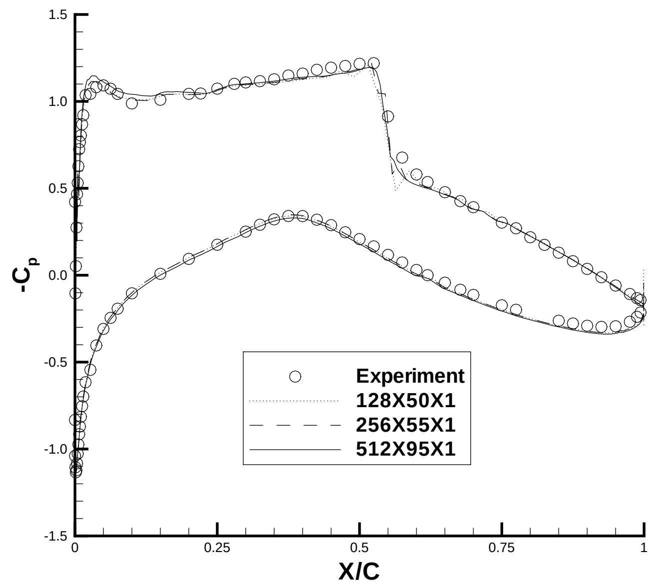

Figure 11: Pressure coefficient comparison

Table 2: Aerodynamic coefficients and $y+$ for RAE 2822 Airfoil

Mesh Dimension	C_d	C_l	C_m	$y+$
128×50	0.01475	0.73790	0.09912	0.0304 - 2.4070
256×55	0.01484	0.74036	0.09914	0.1813 - 2.3649
512×95	0.01354	0.74929	0.09861	0.0559 - 1.7569
Prananta et al.	0.01500	0.74800	0.09800	
Experiment	0.01270	0.74300	0.09500	

Forced Pitching NACA 64A010 Airfoil

Re=1.256×10^7, M_∞=0.8

$$\alpha(t) = \alpha_m + \alpha_o sin(\omega t) \tag{35}$$

$\alpha_m = 0$, $\alpha_o = 1.01°$

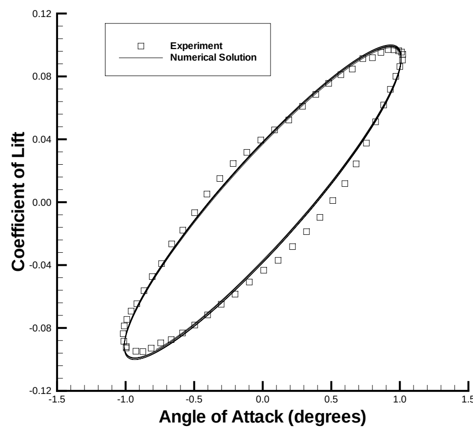

Figure 12: Comparison of computed lift coefficient with Davis' experimental data for the forced pitching airfoil.

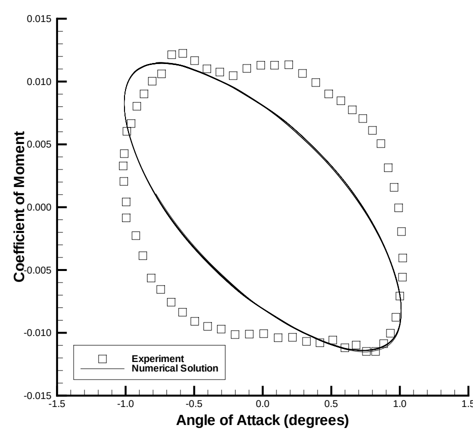

Figure 13: Comparison of computed moment coefficient with Davis' experimental data for the forced pitching airfoil.

Flutter Prediction for NACA 64A010 Airfoil

$Re = 1.256 \times 10^7$, $M_\infty = 0.75 - 0.95$, $a = -2.0$, $x_\alpha = 1.8$, $\frac{\omega_\alpha}{\omega_h} = 1$, $r_\alpha^2 = 3.48$, $\mu = 60$.

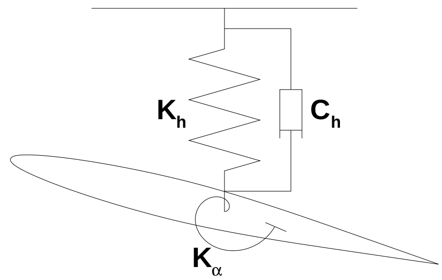

Figure 14: Sketch of the elastically mounted airfoil

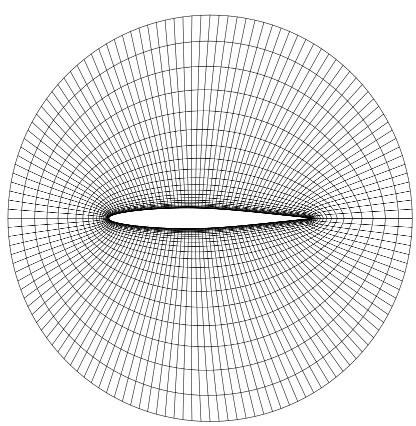

Figure 15: O-type mesh around the NACA 64A010 airfoil

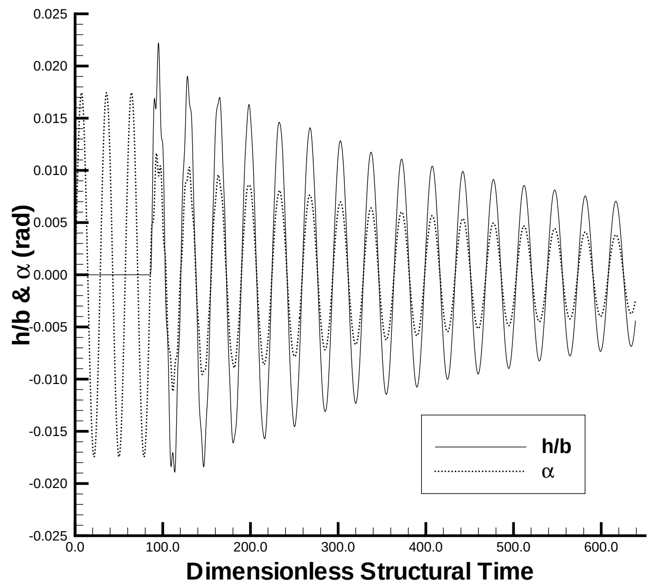

Figure 16: Time histories of plunging and pitching displacements for $M_\infty = 0.825$ and $V^* = 0.55$ - Damped response.

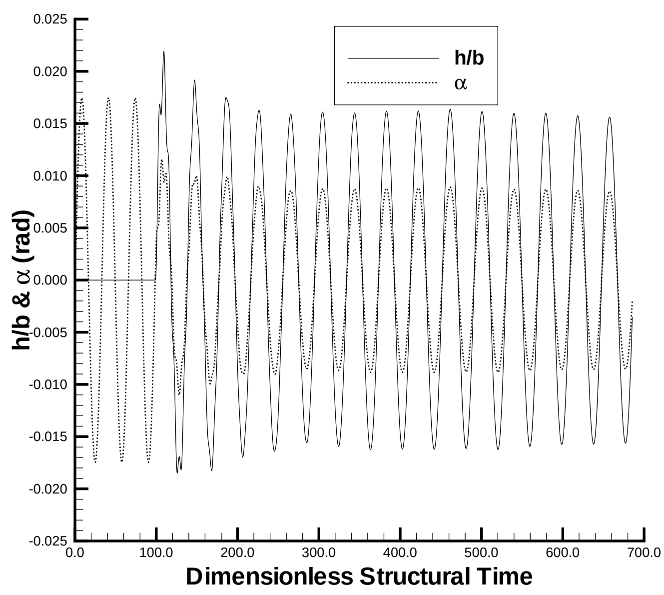

Figure 17: Time histories of plunging and pitching displacements for $M_\infty = 0.825$ and $V^* = 0.59$ - Neutrally stable response.

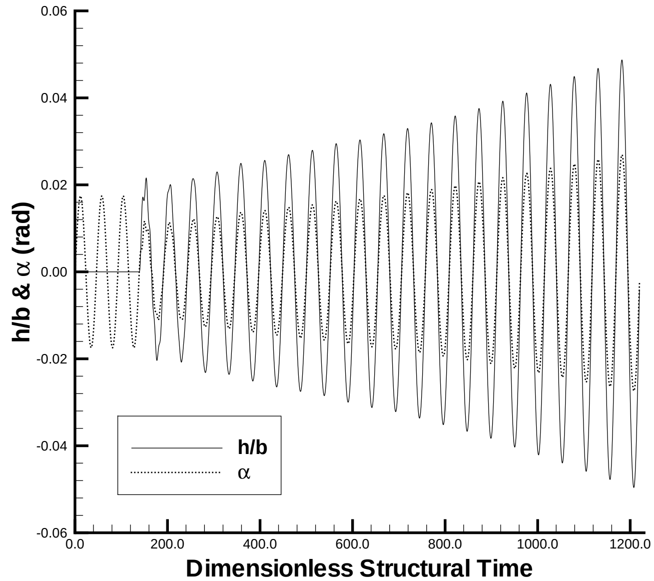

Figure 18: Time histories of plunging and pitching displacements for $M_\infty = 0.825$ and $V^* = 0.70$ - Diverging response.

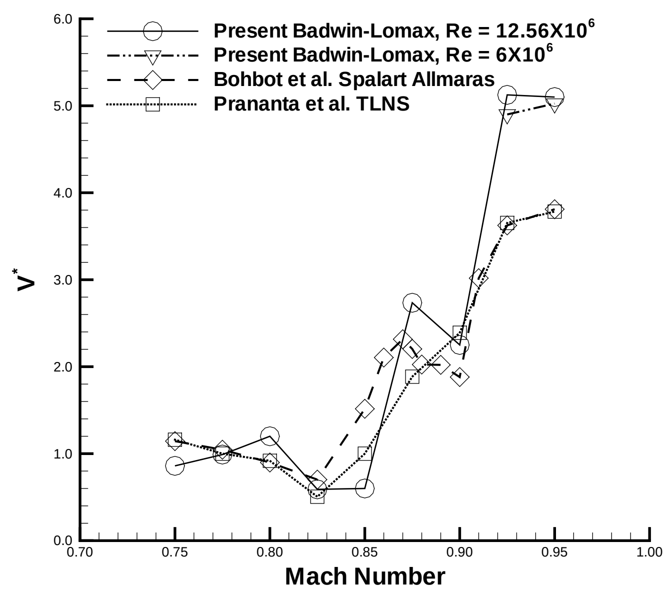

Figure 19: Comparison of computed flutter boundaries - Speed index versus Mach number.

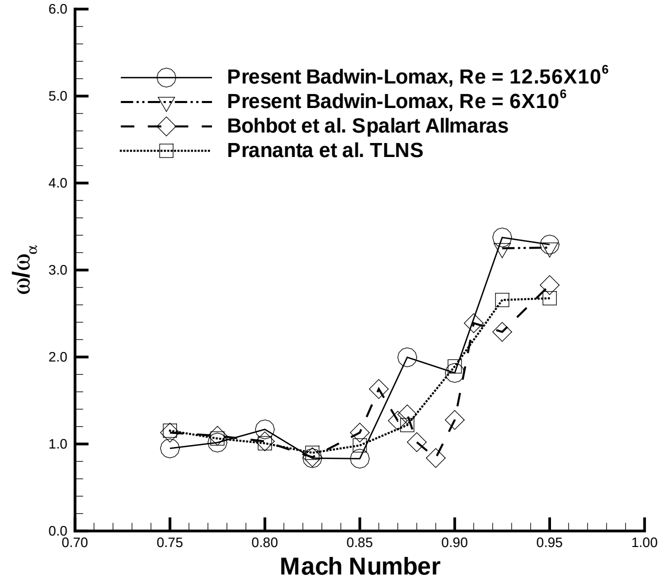

Figure 20: Comparison of computed flutter boundaries - $\frac{\omega}{\omega_\alpha}$ versus Mach number.

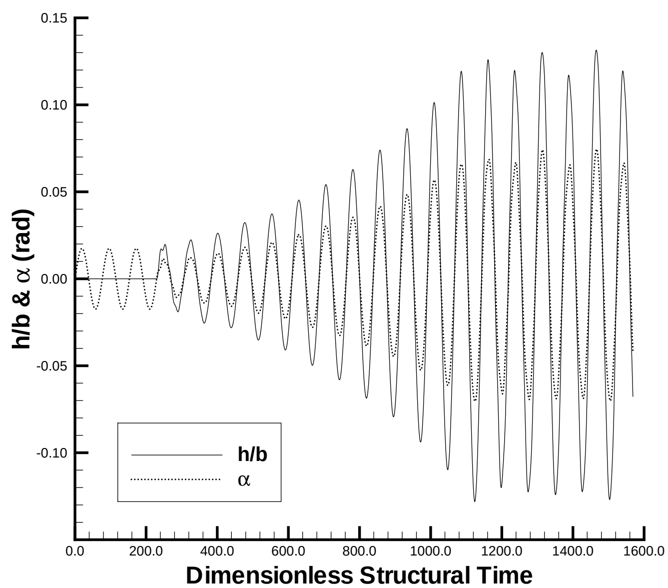

Figure 21: Time histories of plunging and pitching displacements for $M_\infty = 0.825$ and $V^* = 0.9$ - Limit Cycle Oscillation.

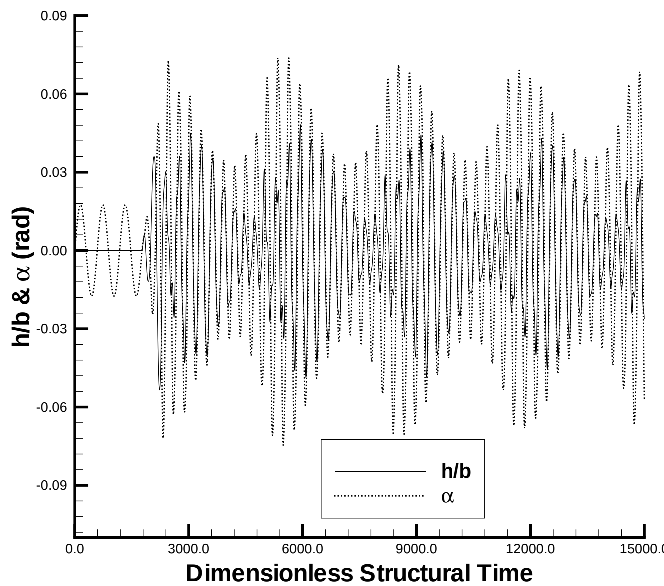

Figure 22: Time histories of plunging and pitching displacements for $M_\infty = 0.9$ and $V^* = 2.5$ - Second mode oscillation.

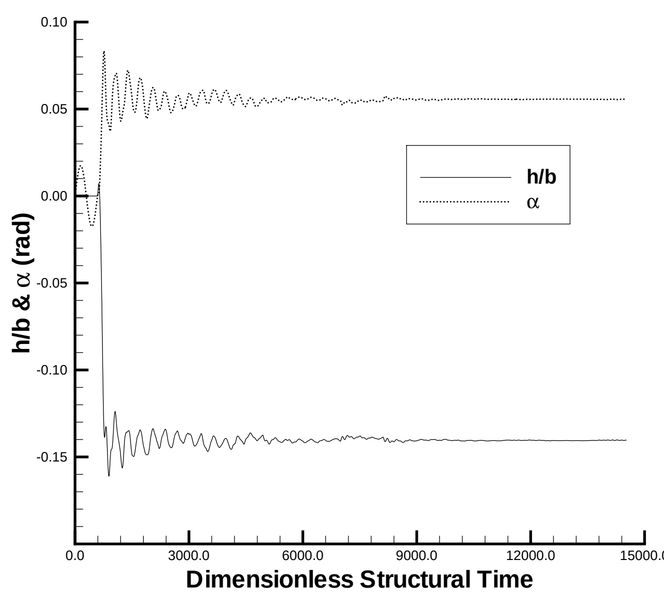

Figure 23: Time histories of plunging and pitching displacements for $M_\infty = 0.875$ and $V^* = 2.5$ - 'Standing' status.

Conclusion

• A fully coupled methodology is developed for calculating the flow-structure interaction problems with moving and deforming mesh systems

• The moving mesh and mesh deformation strategy is based on two mesh zones

• For an elastically mounted cylinder, computed cross-flow displacement of the cylinder agree well with experiment

• For the forced pitching NACA 64A010 airfoil, the computed lift oscillation agrees very well with the experiment The computed moment oscillation has large deviation from the experiment

• For the elastically mounted airfoil, the flutter boundary and the transonic dip agree well with the results of other researchers

• The other phenomena captured in the computations of elastical airfoil include the limit cycle oscillation (LCO) and the steady state flow conditions